CrossMark

Tunable Salisbury Screen Absorber Using Square Lattice of Plasmonic Nanodisk

Adnan Daud Khan[1] · Muhammad Amin[2]

Abstract We propose a novel polarization independent Salisbury screen absorber to provide tunable resonant absorption at terahertz (THz) frequencies. The Salisbury screen absorber is designed by using a planar array of thin gold nanodisks arranged in a square lattice. Certain configurations of Salisbury screen have multiple distinctive absorption bands that support near-unity/FWHM absorption bandwidth reaching 36 THz/169 THz, respectively. Moreover, the absorption bandwidth depends upon the optical thickness of the dielectric spacer between the metasurface and the metallic ground plane. The proposed tunable Salisbury screen absorber can find practical applications in photonic detection, imaging, sensing, and solar cells at optical frequencies.

Introduction

The ability to get broadband absorption of electromagnetic radiation at optical frequencies is often desirable for energy harvesting [1], stealth [2], photo-detection [3], and imaging [4] applications. Several mechanisms are described for electromagnetic absorption, and the most commonly used method is to use metamaterial-based perfect absorbers [5]. Various metamaterial designs are reported that work across a wide range of electromagnetic spectrum from microwave to optical frequencies [5], where the metamaterial absorber is used as a patterned metal surface also known as Salisbury screen to provide complete absorption of light within a given spectrum. The thin absorbing surface placed over a reflecting ground plane separated by a dielectric spacer achieves near-perfect absorption of light.

The operational principle behind the maximal absorption is the destructive interference effect in the multiple reflections from the adjacent interfaces of a metamaterial alike the quarter-wave plate used in the antireflection coatings [6]. The ground reflecting plane prohibits the transmittance ($T = 0$) through the absorber, and the only possible reflection path is suppressed through the coherent reflection cancelation leading to enhancement of absorption within the thin lossy metasurface [7]. Equivalently, the perfect absorption is also described in terms of engineered impedance matching between effective homogeneous medium forming metasurface with substrate and background medium usually air, i.e., ($Z_{eff} = \mu_{eff}/\varepsilon_{eff} = Z_{air}$), where the impedance matching minimizes the reflectance [8].

Metamaterial-based absorbers mostly suffer from bandwidth limitations due to their resonant nature. To overcome this problem, multiple bands of operation are desirable to cover a broad spectral range. This is only possible if multiple resonances are induced on a metasurface screen. Collectively, these resonances offer a broadband absorption of electromagnetic fields. There are several mechanisms described in the literature to get multiple localized surface plasmon resonances [9–12].

✉ Adnan Daud Khan
  adnandaudkhan@gmail.com

1 Department of Electrical Engineering, Sarhad University of Science and Information Technology, LandiAakhun Ahmad, Ring Road, 25000 Peshawar, Pakistan

2 College of Engineering, Taibah University, University Road, 344, Madinah, Saudi Arabia

In this work, we propose a novel Salisbury screen to provide broadband resonant absorption at infrared frequencies. The lossy top metasurface works as a partial reflector. The overall absorption is dependent upon the resonances due to metasurface and the interference between adjacent reflectors. Remarkably, the resonances due to the metasurface can be tuned and optimized to get broadband absorption of light at terahertz frequencies.

Absorber Structure

The top metasurface of the absorber consists of square lattice of gold disks. A schematic view of the unit cell is provided in Fig. 1 having four different nanodisks each with a variable radius ($r_{i = 1–4}$). Such metasurface has been investigated for electromagnetically induced transparency (EIT) recently [13]. Periodic boundary conditions are used to repeat the unit cell along the x- and y-axes. Here, the unit cell period is $p = 266$ nm. Plane wave is normally incident on the metasurface lying on top of a substrate of thickness 'd' followed by gold back reflector. The middle substrate layer provides the necessary multi-reflection resonance path necessary for destructive interference. The square lattice of gold disks helps to induce broadband resonances over the top metasurface. Altogether with the interference from the middle substrate layer, broadband multi-resonance light absorption can be achieved.

Results and Discussion

To achieve a broadband resonant response, periodic disorders are incorporated inside the unit cell of a metasurface. Such periodic disorders can be added either by varying geometry of the nanodisk or by using different materials, e.g., silver and copper. Here, we only varied the radius of each nanodisk to introduce such disorders. These geometrical variations will alter the resonances due to individual nanodisks and the coupling among them. The objective is to design a partially reflecting and dispersive mirror in order to get broadband absorption.

There are several combinations for incorporating defects inside the square lattice of nanodisks (see Fig. 2). These combinations can be divided into four different categories. The first category corresponds to the defectless (symmetric) case having equal radius for all the nanodisks. Further categories refer to one, two, and three defects incorporated inside the unit cell (see Fig. 2). The radius of individual nanodisk inside the square lattice is described as a fraction of parameter $r = 0.22p$, i.e., the unit cell consists of four nanodisks each with a radius $r_{i = 1–4}$ (where $r = 0.22p$) arranged in a square lattice. A 2×2 scaling matrix $S = \begin{bmatrix} a_{11} & a_{12} \\ a_{21} & a_{22} \end{bmatrix}$ in Fig. 2 refers to the scaling used in the radius of nanodisks to incorporate disorder, i.e., $\begin{bmatrix} r_1 & r_2 \\ r_3 & r_4 \end{bmatrix} = \frac{1}{\max(a_{ij})} \begin{bmatrix} ra_{11} & ra_{12} \\ ra_{21} & ra_{22} \end{bmatrix}$ [13]. It can be noted that the optical response of the metasurface will be polarization independent only if the diagonal elements of the scaling matrix ($a_{11} = a_{22}$) are identical.

Defectless Category

To understand the resonant response in each of these cases, we find the individual reflectance characteristics of the standalone square array of plasmonic nanodisks. Here, we consider only the unique combinations with respect to incident polarization. In the defectless category $\left(S = \begin{bmatrix} 1 & 1 \\ 1 & 1 \end{bmatrix} \right)$, the top metasurface is composed of a nanodisk with identical geometric radius. Due to symmetry of the structure, its response is polarization

Fig. 1 A schematic view of the metamaterial unit cell is provided. The top metasurface is followed by a substrate and gold reflector. The thickness of the metasurface is 10 nm. The period of the unit cell is $p = 266$ nm. The metasurface unit cell consists of four gold nanodisks each with a radius ($r_{i = 1–4}$) arranged in a square lattice. Refractive index of substrate is $n = 1.5$
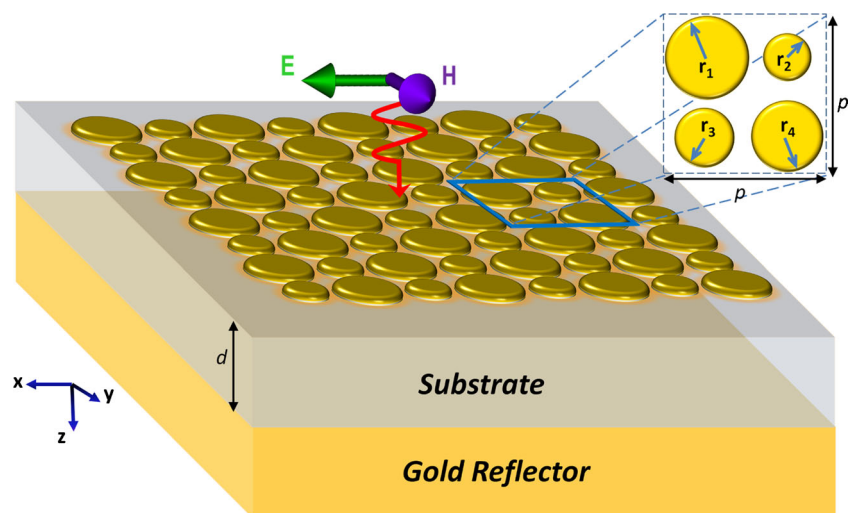
Fig. 2 Reflectance characteristics of a standalone square array of plasmonic nanodisk. The *blue line* corresponds to the polarization-independent case, whereas the *red/green lines* correspond to *x/y* polarizations cases, respectively. All unique configurations are considered for multi-defects incorporated inside the unit cell. The *inset* shows the scaling configuration for the disk radius in a square lattice. Here, the disk radius is scaled inside the unit cell described by a 2×2 square matrix (S)
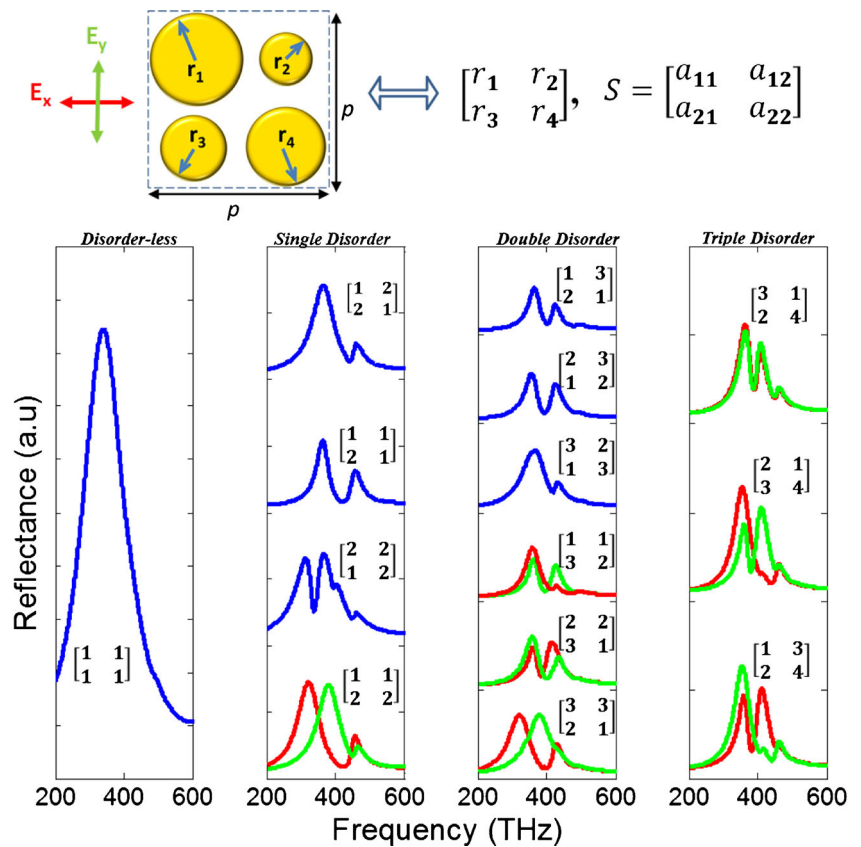
independent and the metasurface exhibits a broad Lorentzian resonance around 350 THz (see Fig. 2).

Single Defect Category

Next, a single defect category is considered, which consists of nanodisks having two different radii (see Fig. 2). There are various ways to place defect into the square lattice: however, only four unique combinations are possible with respect to incident polarization. It can be noted that three out of these four combinations are polarization independent (see Fig. 2).

We first consider the single defect category, which consists of $S = \begin{bmatrix} 1 & 1 \\ 2 & 2 \end{bmatrix}$ (see Fig. 2). Here, the symmetry of the metasurface is relaxed, which makes its response polarization dependent. For *x*-polarized incident light, we get a broad resonant mode near 320 THz and a narrow higher-order mode near 460 THz. The coupling and interference of the two resonant modes results in a sharp Fano asymmetric line shape (see Fig. 2, red curve) [14, 15]. Likewise, for *y*-polarized incident light, we obtained transverse resonant plasmonic modes (see Fig. 2, green curve).

For the single defect type $S = \begin{bmatrix} 1 & 1 \\ 2 & 1 \end{bmatrix}$, and $S = \begin{bmatrix} 1 & 2 \\ 2 & 1 \end{bmatrix}$, the similar broad and narrow hybridized modes are obtained in

the spectrum. However, in contrast to the previous combination, here both the arrangements are polarization independent (diagonal elements are same). The defect type $S = \begin{bmatrix} 2 & 2 \\ 1 & 2 \end{bmatrix}$ is also polarization independent and exhibits multiple higher-order modes. This arrangement is most significant compared to the previous cases because it induces several Fano asymmetric line shapes and it may be beneficial for creating a dispersive partially reflecting mirror.

Twin Defect Category

The twin defect category consists of two defects (having three different radii) inside the unit cell. It can be noted that this category consists of six unique combinations with respect to incident polarization. Moreover, three out of these combinations are polarization independent, i.e., $S = \begin{bmatrix} 1 & 3 \\ 2 & 1 \end{bmatrix}$, $S = \begin{bmatrix} 2 & 3 \\ 1 & 2 \end{bmatrix}$, and $S = \begin{bmatrix} 3 & 2 \\ 1 & 3 \end{bmatrix}$, respectively (see Fig. 2). It appears that most of these cases exhibit first-order broad and higher-order narrow hybridized modes that in turn induce a single asymmetric Fano line shape. These combinations are significant because it is expected that such arrangements will prove to be beneficial for creating a dispersive partially reflecting mirror.

Triple Defect Category

The triple defect category consists of three defects (having four different radii) inside the unit cell, i.e., all the entities of this unit cell are dissimilar. Obviously, this leads to three unique combinations with respect to incident field polarization. However, due to dissimilarity of these nanodisks, all of three combinations are polarization dependent (see Fig. 2). Here, multiple higher-order hybridized modes and asymmetric line shapes arise for x- and y-polarized $S = \begin{bmatrix} 3 & 1 \\ 2 & 4 \end{bmatrix}$, y-polarized $S = \begin{bmatrix} 2 & 1 \\ 3 & 4 \end{bmatrix}$, and x-polarized $S = \begin{bmatrix} 1 & 3 \\ 2 & 4 \end{bmatrix}$ categories. We will further investigate the perfect absorption properties using such categories.

Perfect Absorber

In this section, we merge the collective properties due to metasurface screen and the ground reflector separated by a dielectric spacer. The setup of the perfect absorber is shown in Fig. 1, where the bottom gold reflector is used to completely eliminate the transmittance for the whole spectrum and the middle dielectric spacer between the metasurface and gold reflector works as a resonator. The optimized absorptivity spectra can be calculated using $A(\omega) = 1 - R(\omega) - T(\omega)$, where $T(\omega) \approx 0$ due to the gold reflector. So, the overall expression is

$$A = 1 - \left| S_{11} + \frac{S_{21}S_{12}S_{22}e^{-i2\phi_1}}{1 - S_{11}S_{22}e^{-i2\phi_1}} \right|^2 \tag{1}$$

Here, $\phi_1 = 2nd$ is phase length due to a dielectric spacer medium between metasurface and ground plane and n is their refractive index. S_{ij} are two-port scattering parameters along each port direction i, given the incident wave is from port j. The scattering parameters are evaluated using full wave electromagnetic solver. The role of back reflector is analytically solved by utilizing appropriate boundary conditions using Eq. (1).

The dielectric spacer layer could be thought of as a Fabry-Perot interferometer terminated at its ends with a reflective gold ground plane and a partially reflective metasurface [9]. In laser physics, the free spectral range $FSR = c/2nd$ and finesse = FSR/FWHM represent the frequency difference between successive resonant transmission peaks and sharpness of the resonance peaks, respectively [9]. Similar to this concept, here the FSR and finesse of the dielectric layer determine its absorption properties in the resonator. However, unlike a laser mirror cavity, the dielectric layers represent a dispersive and lossy cavity, since it is terminated by a lossy gold metasurface. Clearly, d should be selected carefully, since it determines the resonance locations where we achieved perfect absorption, i.e., $A \approx 1$. It also has an effect on the bandwidth of absorption, since the metasurface support two resonant peaks in the reflectance spectrum with different bandwidths.

It is to be noted that only polarization-independent metasurfaces are chosen for broadband absorber application [11, 16, 17]. The full width at half maximum (FWHM) is calculated for various cases. By using such method, it appears that almost all of the polarization-independent metasurface combinations given in Fig. 2 exhibit a resonant response in the absorption spectrum. However, it must be noted here that

Table 1 Comparison between bandwidths of 50 % absorption at terahertz frequencies

Type	FWHM absorption bandwidth	Normalized BW/$f_0 \times 100$	d (nm)
$S = \begin{bmatrix} 1 & 1 \\ 1 & 1 \end{bmatrix}$	555.4 − 477.7 THz = 77.7 THz	15.04	116
$S = \begin{bmatrix} 2 & 2 \\ 1 & 2 \end{bmatrix}$	350.5 − 323.4 THz = 27.1 THz 492.1 − 388.3 THz = 103.8 THz	8.04, 23.6	141
$S = \begin{bmatrix} 1 & 1 \\ 2 & 1 \end{bmatrix}$	514.5 − 345.5 THz = 169 THz	39.3	112
$S = \begin{bmatrix} 1 & 2 \\ 2 & 1 \end{bmatrix}$	552.4 − 433.8 THz = 118.6 THz	24.1	101
$S = \begin{bmatrix} 3 & 2 \\ 1 & 3 \end{bmatrix}$	502.6 − 399.3 THz = 103.3 THz	22.9	131
$S = \begin{bmatrix} 2 & 3 \\ 1 & 2 \end{bmatrix}$	515.1 − 353.8 THz = 161.3 THz	37.1	120
$S = \begin{bmatrix} 1 & 3 \\ 2 & 1 \end{bmatrix}$	516.3 − 350.3 THz = 166 THz	38.3	113
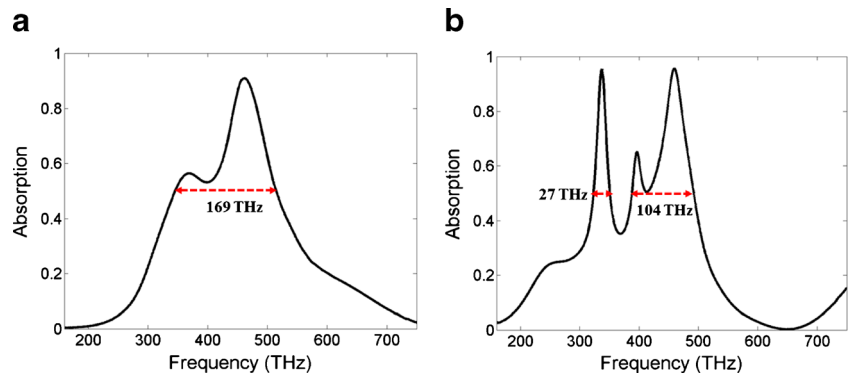
thickness of substrate is the most important parameter that controls the bandwidth of absorption.

FWHM Bandwidth of Absorption

A comparison between normalized bandwidth of absorption for the various polarization-independent cases is in shown in Table 1. The most important Salisbury screen is $S = \begin{bmatrix} 1 & 1 \\ 2 & 1 \end{bmatrix}$, where the bandwidth of 50 % absorption reaches approximately 169 THz making the absorber suitable for practical applications. The absorption spectra of such metasurface is shown in Fig. 3a, where the value of d is selected as 112 nm. The metasurface type $S = \begin{bmatrix} 2 & 2 \\ 1 & 2 \end{bmatrix}$ supports dual bands, where the bandwidth of 50 % absorption reaches approximately 103.8 and 27.1 THz, respectively, at $d = 141$ nm (see Fig. 3b). Such Salisbury screen is a perfect option for solar cell applications [11, 17].

Bandwidth of Perfect Absorption

The absorption above 90 % of the metasurfaces given in Fig. 2 are also evaluated (see Table 2). The most significant

Salisbury screen is $S = \begin{bmatrix} 1 & 1 \\ 2 & 1 \end{bmatrix}$, where twin absorption resonances are obtained above 90 %. The absorption spectra of such metasurface, where the value of d is selected as 934 nm, is shown in Fig. 4. The broad absorption bandwidth reaches approximately 36 THz at 459 THz, and the electromagnetic wave energy of 98.7 % is absorbed at 446 THz and 98.5 % at 472 THz, respectively. There is also a narrow band peak around 379 THz with an absorption bandwidth of 6.6 THz, and the absorption efficiency is 99.99 %. This narrow band is less significant as it does not absorb many frequencies of electromagnetic wave, but it is definitely used for sensing purposes at visible frequencies. It can be noted that large length of spacer layer $d = 934$ nm means the FSR is clearly visible, i.e., FSR = 107 THz.

Conclusion

The Salisbury screen absorber, which consists of a planar array of thin gold nanodisks arranged in a square lattice, providing wide-band perfect absorption at terahertz frequencies is analyzed theoretically. The near-perfect absorptions are obtained above 50 and 90 % absorption with absorption

Table 2 Comparison between bandwidths of 90 % absorption at terahertz frequencies

Type	Absorption bandwidth	Normalized BW/ $f_0 \times 100$	d (nm)
$S = \begin{bmatrix} 2 & 2 \\ 1 & 2 \end{bmatrix}$	$414.3 - 391$ THz $= 23.3$ THz	5.8	182
$S = \begin{bmatrix} 1 & 1 \\ 2 & 1 \end{bmatrix}$	$476.8 - 440.8$ THz $= 36$ THz $382.4 - 375.8$ THz $= 6.6$ THz	7.9, 1.7	934
$S = \begin{bmatrix} 1 & 2 \\ 2 & 1 \end{bmatrix}$	$473.8 - 445.3$ THz $= 28.5$ THz	6.2	335
$S = \begin{bmatrix} 3 & 2 \\ 1 & 3 \end{bmatrix}$	$440.6 - 409.6$ THz $= 31$ THz	7.3	156
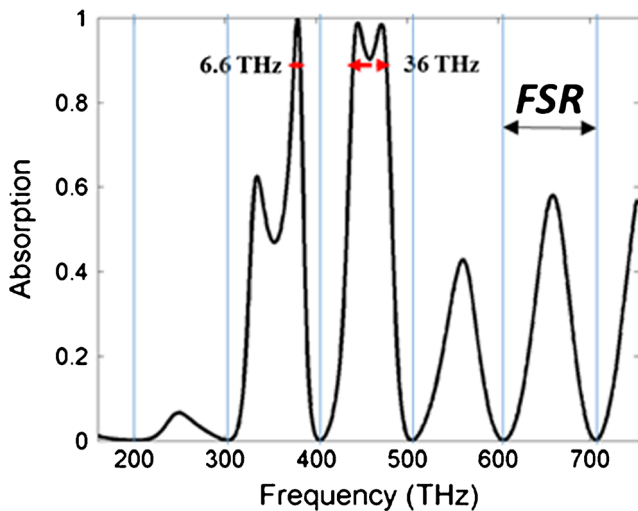
Fig. 4 Absorption spectra of the metasurface $S = \begin{bmatrix} 1 & 1 \\ 2 & 1 \end{bmatrix}$ with $d = 934$ nm. Here, the multiple peaks are repeating with FSR = 107 THz

bandwidths reaching approximately 169 and 36 THz, respectively. The proposed broadband absorber has potential applications in photonic detection, imaging, and solar cells.

References

1. Guo CF, Sun T, Cao F, Liu Q, Ren Z (2014) Metallic nanostructures for light trapping in energy-harvesting devices. Light: Sci Appl 3(4):e161
2. Iwaszczuk K, Strikwerda AC, Fan K, Zhang X, Averitt RD, Jepsen PU (2012) Flexible metamaterial absorbers for stealth applications at terahertz frequencies. Opt Express 20(1):635–643
3. Zhao F, Zhang C, Chang H, Hu X (2014) Design of plasmonic perfect absorbers for quantum-well infrared photodetection. Plasmonics 9(6):1397–1400
4. Tittl A, Michel AKU, Schäferling M, Yin X, Gholipour B, Cui L, Wuttig M, Taubner T, Neubrech F, Giessen H (2015) A switchable mid-infrared plasmonic perfect absorber with multispectral thermal imaging capability. Adv Mater 27(31): 4597–4603
5. Watts CM, Liu X, Padilla WJ (2012) Metamaterial electromagnetic wave absorbers. Adv Mater 24(23):OP98–OP120
6. Baryshnikova K, Petrov M, Babicheva V, Belov P (2015) Plasmonic and silicon spherical nanoparticle anti-reflective coatings. arXiv preprint arXiv:150806578
7. Chen H-T (2012) Interference theory of metamaterial perfect absorbers. Opt Express 20(7):7165–7172
8. Tao H, Landy NI, Bingham CM, Zhang X, Averitt RD, Padilla WJ (2008) A metamaterial absorber for the terahertz regime: design, fabrication and characterization. Opt Express 16(10):7181–7188
9. Amin M, Farhat M, Bağcı H (2013) An ultra-broadband multilayered graphene absorber. Opt Express 21(24):29938–29948
10. Wang J, Fan C, Ding P, He J, Cheng Y, Hu W, Cai G, Liang E, Xue Q (2012) Tunable broad-band perfect absorber by exciting of multiple plasmon resonances at optical frequency. Opt Express 20(14): 14871–14878
11. He X, Yan S, Lu G, Zhang Q, Wu F, Jiang J (2015) An ultra-broadband polarization-independent perfect absorber for the solar spectrum. RSC Adv 5(76):61955–61959
12. Li W, Valentine J (2014) Metamaterial perfect absorber based hot electron photodetection. Nano Lett 14(6):3510–3514
13. Amin M, Khan AD (2015) Polarization selective electromagnetic-induced transparency in the disordered plasmonic quasi-crystal structure. J Phys Chem C
14. Khan AD, Miano G (2013) Plasmonic Fano resonances in single-layer gold conical nanoshells. Plasmonics 8(3):1429–1437
15. Khan AD, Khan SD, Khan R, Ahmad N, Ali A, Khalil A, Khan FA (2014) Generation of multiple Fano resonances in plasmonic split nanoring dimer. Plasmonics 9(5):1091–1102
16. Wang B, Zhai X, Wang G, Huang W, Wang LL (2015) Design of a four-band and polarization-insensitive terahertz metamaterial absorber. Photon J, IEEE 7(1):1–8
17. Rufangura P, Sabah C (2015) Dual-band perfect metamaterial absorber for solar cell applications. Vacuum 120:68–74